Comparison of Multiexcitation Fluorescence and Diffuse Reflectance Spectroscopy for the Diagnosis of Breast Cancer (March 2003)

Gregory M. Palmer, Changfang Zhu, Tara M. Breslin, Fushen Xu, Kennedy W. Gilchrist, and Nirmala Ramanujam*

***Abstract*—Nonmalignant ($n = 36$) and malignant ($n = 20$) tissue samples were obtained from breast cancer and breast reduction surgeries. These tissues were characterized using multiple excitation wavelength fluorescence spectroscopy and diffuse reflectance spectroscopy in the ultraviolet-visible wavelength range, immediately after excision. Spectra were then analyzed using principal component analysis (PCA) as a data reduction technique. PCA was performed on each fluorescence spectrum, as well as on the diffuse reflectance spectrum individually, to establish a set of principal components for each spectrum. A Wilcoxon rank-sum test was used to determine which principal components show statistically significant differences between malignant and nonmalignant tissues. Finally, a support vector machine (SVM) algorithm was utilized to classify the samples based on the diagnostically useful principal components. Cross-validation of this nonparametric algorithm was carried out to determine its classification accuracy in an unbiased manner. Multiexcitation fluorescence spectroscopy was successful in discriminating malignant and nonmalignant tissues, with a sensitivity and specificity of 70% and 92%, respectively. The sensitivity (30%) and specificity (78%) of diffuse reflectance spectroscopy alone was significantly lower. Combining fluorescence and diffuse reflectance spectra did not improve the classification accuracy of an algorithm based on fluorescence spectra alone. The fluorescence excitation-emission wavelengths identified as being diagnostic from the PCA-SVM algorithm suggest that the important fluorophores for breast cancer diagnosis are most likely tryptophan, NAD(P)H and flavoproteins.**

***Index Terms*—Breast cancer, fluorescence, reflectance, spectroscopy.**

I. Introduction

BREAST cancer screening relies on mammography and clinical breast exam for identifying suspicious lesions. Mammograms are useful in detecting small tumors that may be unnoticeable by physical exam; however, they produce a significant percentage of false positives [1]. As a result, follow up diagnostic procedures such as percutaneous needle biopsy are performed to further evaluate breast abnormalities [1]. Needle biopsy has a limited sampling accuracy because only a few small pieces of tissue are extracted from random locations in the suspicious mass. In some cases, sampling of the suspicious mass may be missed altogether. Consequences include a false-negative rate of 1%–7% [2] when verified with follow up mammography, as well as the requirement of repeat biopsies (percutaneous or surgical) in 9%–18% of patients [3], [4] (due to discordance between histological findings and mammography).

Optical sensors based on ultraviolet-visible (UV-VIS) spectroscopy have the potential to improve the sampling accuracy of core needle biopsy by enabling sampling of multiple tissue sites without the need for biopsy, and by providing real-time diagnosis. Fluorescence and diffuse reflectance spectroscopic measurements in the UV-VIS have been shown to have consistently high sensitivities and specificities for detecting human pre-cancers and cancers, *in vivo* in a number of organ sites including the gastrointestinal tract, bronchus, and cervix [5]. Additionally, several groups have demonstrated that there are significant differences in the fluorescence and diffuse reflectance spectra of normal, benign and malignant breast tissues [6]–[16]. Incorporating UV-VIS spectroscopy as an adjunct diagnostic modality to core needle biopsy could potentially reduce the false negative rate of current needle biopsy procedures. This in turn could potentially lead to fewer repeat biopsies in patients with suspicious breast lesions.

The endogenous fluorophores present in breast tissue include tryptophan, reduced nicotinamide adenine dinucleotide (phosphate) (NAD(P)H), flavin adenine dinucleotide (FAD), and collagen [17]. Tryptophan fluorescence, which has an excitation, emission maximum of 300, 340 nm, is an indicator of protein or free tryptophan content. NAD(P)H and flavoproteins are indicators of metabolic activity [17] and have excitation, emission maxima at 351, 460 nm and 450–520 nm, respectively [17]. Collagen is the primary structural protein in the extracellular matrix. It has several excitation, emission maxima, one of which occurs at 325, 390 nm (due to cross-link fluorescence) [17].

Alfano *et al.* [12] were the first to measure fluorescence spectra of malignant and nonmalignant breast tissues. Since then, several groups have investigated the use of fluorescence spectroscopy for breast cancer detection in *ex vivo* studies [6]–[12]. In the collective set of studies to date, emission spectra were acquired at excitation wavelengths of 300, 340,

Manuscript received November 13, 2002; revised March 1, 2003. This work was supported by the Whitaker Foundation and the U.S. Department of Defense Breast Cancer Research Project. *Asterisk indicates corresponding author.*

G. M. Palmer is with the Department of Biomedical Engineering at the University of Wisconsin, Madison, WI 53706 USA (e-mail: gmpalmer@wisc.edu).

C. Zhu is with the Department of Electrical and Computer Engineering at the University of Wisconsin, Madison, WI 53706 USA (e-mail: czhu@cae.wisc.edu).

F. Xu and K. W. Gilchrist are with the Department of Pathology at the University of Wisconsin Medical School, WI 53706 USA (e-mail: fushenxu@hotmail.com; kwgilchr@facstaff.wisc.edu).

T. M. Breslin is with the Department of Surgery at the University of Wisconsin School of Medicine, WI 53706 USA (e-mail: breslin@surgery.wisc.edu).

*N. Ramanujam are with the Department of Biomedical Engineering at the University of Wisconsin, Madison, WI 53706 USA (e-mail: nimmi@engr.wisc.edu).

Digital Object Identifier 10.1109/TBME.2003.818488

458, 488, and 514 nm and excitation spectra were measured at emission wavelengths of 340, 390, and 460 nm from, normal, benign, and malignant breast tissues. Emission spectroscopy measures the fluorescence spectrum, while excitation spectroscopy measures the absorption spectrum of a fluorophore. The wavelength-dependent effects of nonfluorescent absorbers and scatterers in tissue also affect the tissue excitation and emission spectra.

Gupta [7] and Majumder *et al.* [6] analyzed different data sets collected from the same set of breast tissues *ex vivo* and showed that the emission spectra at excitation wavelengths of 340 and 488 nm and excitation spectra at emission wavelengths 390 and 460 nm exhibit significant differences between normal, benign and malignant tissues. Using the integrated emission intensities at an excitation wavelength of 340 nm, in a binary classification scheme, they were able to differentiate malignant from normal and benign tissues with a sensitivity and specificity of 98%. The fluorescence was attributed to reduced nicotinamide adenine dinucleotide (NADH) and collagen. Yang *et al.* [8]–[10] reported that emission spectra at 300-nm excitation and excitation spectra at 340-nm emission (tryptophan is the primary fluorophore) can separate malignant and nonmalignant tissues. They found, for example, that the ratio of normalized intensities at 289 and 268 nm of the excitation spectra discriminate between malignant and fibrous tissues with 93% sensitivity and 95% specificity. Although previous work shows promising results, there are important gaps in these studies that still need to be addressed. The main limitations of previous studies are: 1) fluorescence spectra were obtained only at one or several excitation wavelengths from breast tissues; 2) the utility of combining fluorescence and diffuse reflectance spectroscopy was not evaluated; and 3) the classification accuracy of the diagnostic algorithms were not tested in an unbiased manner.

Spectral differences observed in the fluorescence spectra of normal, benign and malignant breast tissues can also be attributed in part to nonfluorescent absorbers and scatterers. Diffuse reflectance spectroscopy provides a direct measurement of tissue absorption as well as scattering. The primary nonfluorescent absorbers in the UV-VIS in breast tissue are DNA, oxygenated and deoxygenated hemoglobin and β-carotene [18].

Several groups have explored the utility of diffuse reflectance spectroscopy between 250–800 nm, for breast cancer detection *ex vivo* [10], [13]–[15] and *in vivo*[15], [16]. Bigio *et al.* [16] measured diffuse reflectance spectra through a core biopsy needle and during breast cancer surgery and showed that this technique can differentiate malignant from normal tissues with a sensitivity of 60%–70% and a specificity of 85%–95%. The collective set of *ex vivo* and *in vivo* studies [10], [13]–[16] show that diffuse reflectance spectra can differentiate malignant from normal tissues. The changes in the diffuse reflectance of malignant tissues, was attributed to increased DNA, protein and hemoglobin absorption and increased scattering.

The primary goal of the study described here was to characterize the multiexcitation fluorescence spectra (at a total of nine excitation wavelengths in the UV-VIS) and UV-VIS diffuse reflectance spectra of malignant and nonmalignant breast tissues and to identify the optimal spectral features for breast cancer diagnosis. A novel nonparametric algorithm (applicable for small sample sizes) was developed to analyze the breast tissue fluorescence and diffuse reflectance spectra in order to classify a particular sample as malignant or nonmalignant (benign, normal) and a cross-validation scheme was utilized to test the algorithm's classification accuracy in an unbiased manner.

II. Methods

A. Tissue Handling Protocol for Ex Vivo Studies

All of the fluorescence and most of the diffuse reflectance measurements to date have been made on excised breast tissues. However, no systematic investigations have been carried out to assess the effect of excision and time after excision on the tissue fluorescence and diffuse reflectance spectra. Therefore, the effects of tissue handling and storage on optical spectroscopy of excised tissue specimens were systematically evaluated in a previous study [19]. In that study, multiexcitation fluorescence and diffuse reflectance spectra of the epithelial tissue of the hamster cheek pouch was characterized *in vivo*, *ex vivo* (immediately after excision) and after being frozen and thawed. The results indicated that the freezing and thawing process of tissue produces a significant deviation in intensity and line shape relative to the *in vivo* spectra over the entire UV-VIS range. On the other hand, *ex vivo* spectra measured within a short time after excision were found to provide a relatively close approximation of *in vivo* spectra.

B. Optical Spectroscopy of Breast Tissues

Approval for the optical spectroscopy study was obtained from the Institutional Review Board at the University of Wisconsin, Madison. Tissue was obtained from patients undergoing either a lumpectomy, mastectomy or breast reduction surgery. In the routine clinical protocol, tissue specimens were harvested during surgery and normal and tumor tissue samples were cut from the larger specimen. The tissue samples that were cut from the larger specimen were generally at least 1 cm in length/width and 3 mm thick, thus providing a semi-infinite geometry for optical spectroscopy. Optical spectroscopic measurements were carried out on the fresh tissue samples, within two hours after surgical excision. Measurements were made on a total of 56 different tissue samples, from a total of 32 different patients. In the majority of patients who participated in this study, a normal and tumor pair was obtained for optical spectroscopy. When normal and tumor tissue sites were available from a patient, the normal tissue specimen was obtained from the same breast that contained the tumor (bilateral cancer surgeries are relatively rare). In most cases, the normal tissue was obtained as far as possible from the tumor site (generally 1 cm or more from the tumor boundary) in order to minimize the potential effects of malignancy. In a minority of the patients, only either a normal or tumor sample was available for the measurement, usually due to limitations in the size of the surgical specimen.

All measurements were made using a Skinscan spectrofluorometer (JY Horiba, Edison, NJ). This instrument consists of a 150 W xenon lamp, double grating excitation and emission monochromators having fixed bandpasses of 5 nm for both excitation and emission, and a photomultiplier tube (PMT). The adjustable parameters of the system are the wavelength range and increment, the signal acquisition time and the PMT high voltage. The illumination and collection of light was coupled through a fiber optic probe, consisting of a central collection

core with a diameter of 1.52 mm surrounded by an illumination ring, with an outer diameter of 2.18 mm. Both the illumination ring and collection core are made up of 31 individual fibers, each with a core/cladding diameter of 200/245 μm. The numerical aperture of the excitation and emission fibers is 0.125 and 0.12, respectively. The probe geometry was designed to maximize the probing depth in the tissue, while providing good signal-to-noise ratio. Simulations using a modified, three-dimensional, weighted-photon Monte Carlo code have been carried out to evaluate the probing depth achieved with this illumination and collection geometry in a turbid medium [20]. For a homogeneous medium with a fixed scattering coefficient of 110.4 cm^{-1}, and absorption coefficient varying from 31.8 cm^{-1} to 1.3 cm^{-1} (i.e., absorption coefficients spanning the UV-VIS range), the probing depth varied from 450 to 1350 μm. In a turbid medium with a fixed absorption coefficient of 10.8 cm^{-1}, and scattering coefficient varying from 225 cm^{-1} to 50 cm^{-1} (i.e., scattering coefficients spanning the UV-VIS range), the probing depth varied from 550 to 1050 μm. The probing depth in a medium with absorption (2.3 cm^{-1}) and scattering coefficients (167 cm^{-1}) representative of breast adipose tissue at 540 nm [21] was 1050 μm.

Fluorescence emission spectra were recorded at excitation wavelengths of 300 to 460 nm, in 20-nm increments. At each excitation wavelength, fluorescence emission was recorded from 10 nm greater than the excitation wavelength, up to 600 nm, in 5-nm increments (e.g., 310 to 600 nm at an excitation wavelength of 300 nm). Fluorescence emission spectra were obtained at a total of nine excitation wavelengths. A signal acquisition time of 0.5 s was used per excitation-emission wavelength pair and the PMT high voltage was set at 950 V for all measurements. The total measurement time was approximately 8 min. The fluorescence emission spectral intensities at each excitation wavelength were normalized to that of a reference photodiode, which accounts for wavelength-dependent variations of the excitation light intensity. The fluorescence emission spectrum at each excitation wavelength was corrected for wavelength dependencies in the emission monochromator and PMT using instrument specific correction factors. Finally, all fluorescence emission spectral intensities were divided by the peak fluorescence intensity (excitation-emission: 460–575 nm) of a Rhodamine B dye (115H3423, Sigma Chemical Co., MO) dissolved in water (2.14 μM), measured after each patient study to correct for time-dependent changes in the throughput of the instrument.

Diffuse reflectance was measured from 300 to 600 nm. This measurement was made in a synchronous scan mode, whereby the excitation and emission gratings are moved simultaneously. The diffuse reflectance measurements were made at an increment of 5 nm, with a signal acquisition time of 0.1s/wavelength and at a PMT high voltage of 340 or 450 V. The difference in the PMT high voltage is due to two different instruments being used in the course of the study (both identical models), each having slightly different throughputs. The instruments were otherwise identical and were calibrated, such that this difference does not introduce artifacts into the data. The diffuse reflectance spectrum was corrected for the wavelength-dependent system response and the throughput of the instrument by normalizing it to that of a Spectralon 99% reflectance puck (SRS-99–010, Labsphere, Inc., North Sutton, NH), which was measured with the probe in contact with the puck (no coupling media was used).

TABLE I
HISTOLOGICAL BREAKDOWN OF THE 56 BREAST TISSUE SAMPLES EXAMINED IN THE OPTICAL SPECTROSCOPY STUDY

Total Malignant Tissues	**20**
Invasive ductal carcinoma (IDC)	16
Invasive lobular carcinoma	2
Carcinoma in situ (CIS)	1
CIS + IDC combined	1
Total Normal/Benign Fibrous Tissues	**15**
Normal fibrous tissue	8
Adenosis	2
Reparative Changes	2
Fibrocystic disease	1
Fibroadenoma	1
Cystic	1
Total Normal Adipose Tissues	**21**

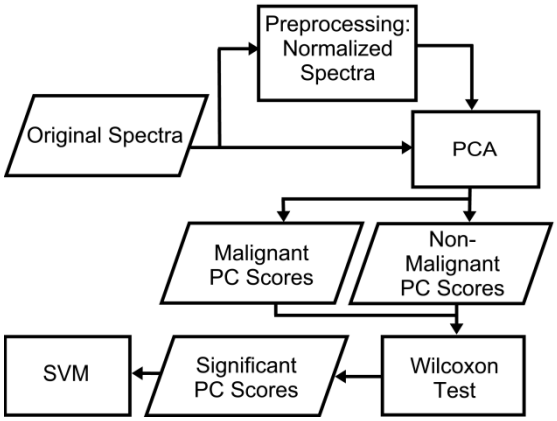

Fig. 1. Flow chart of the algorithm that was developed to analyze breast tissue fluorescence and diffuse reflectance spectra (PCA—principal component analysis; SVM—support vector machine).

After each measurement, the exact site where the probe was positioned on each tissue sample was inked (TMD-BK, Triangle Biomedical Sciences, Durham, NC) and then cut and stained for histopathology. Microscopic evaluation of each histological section was performed (KG, FX) and a consensus diagnosis was reached. When a sample exhibited a heterogeneous diagnosis at the site of measurement, the most severe diagnosis was used (e.g., for samples which had both normal glandular tissue as well as malignant tissue, the sample diagnosis was designated as being malignant). In samples in which both normal adipose and fibroglandular tissues were present, the histology was designated to be that of the predominant tissue type at the site of measurement. Table I shows the histological breakdown of the 56 breast tissue samples examined in the optical spectroscopy study. Eleven of the malignant samples had a histological normal counterpart from the same patient.

C. Data Analysis

Fig. 1 shows the flow chart of the algorithm that was developed to analyze breast tissue fluorescence and diffuse reflectance spectra. Two different types of input data sets were used. In the first case, the original spectra were used. The primary sources of variance in the original spectra are the intensity and spectral line shape. In the second case, each fluorescence

spectrum was normalized to its peak intensity, or in the case of the diffuse reflectance spectrum, to its integrated intensity. The primary source of variance in this case was attributed to the spectral line shape. The benefit of preprocessing by normalization is that it cancels out inter-patient variations in intensity and allows a direct comparison of spectral line shape.

Principal Component Analysis (PCA) was employed as a data reduction technique [22]. PCA characterizes a majority of the variance while greatly reducing the input data set into a few orthogonal variables. The principal components (PCs) are extracted such that the first principal component (PC1) accounts for the largest amount of the total variance of the input data. The second PC (PC2) accounts for the second largest amount of the variance while being orthogonal to PC1, and so on. Thereby PCA projects the set of observed data onto a subspace expanded by the PCs. There are two advantages of this transformation: 1) the input data can be represented by a few subsets of PCs with minimal mean square error, which reduces the dimensionality of the data set; 2) the projection onto the PC subspace maximizes the separation of data clusters. PCA can be carried out on concatenated spectra (fluorescence emission spectra at all nine excitation wavelengths and diffuse reflectance spectra). Alternatively, PCA can be performed on all fluorescence emission spectra, one excitation wavelength at a time and individually on the diffuse reflectance spectra. Both approaches will yield the same set of eigenvectors for each spectrum. However, in the first case, one set of PC scores will be generated for all spectra per sample, whereas in the second case, one set of PCs will be generated for each spectrum per sample. In this study, PCA was performed on all fluorescence emission spectra, one excitation wavelength at a time and separately on the diffuse reflectance spectra to yield a set of PCs for each spectral data set. The subsets of PCs that account for the majority (95% or 99%) of the variance, rather than all of the PCs, were retained for further processing. Using more PCs (99% versus the 95% criterion) retains a greater proportion of the variance of the input data set.

A Wilcoxon rank-sum (unpaired) or rank-signed (paired) test [23] was then employed to determine which PC scores showed statistically significant differences between malignant and nonmalignant tissue types. This particular test was used because it is a nonparametric test, which is appropriate for small sample sizes for which a normal distribution cannot be assumed. Using a standard criterion of $p < 0.05$, PCs from all nine fluorescence spectra and the diffuse reflectance spectrum showed significant differences between malignant and nonmalignant tissues. However, in a clinical setting, it would be desirable to limit the number of measurement parameters (and, thus, the measurement time) required for diagnosis. Thus, PCs that showed differences between malignant and nonmalignant tissue types at varying significance levels of $p < 0.05$, $p < 0.005$ and $p < 0.0005$ were retained as inputs into the classification scheme. This was carried out to evaluate the classification accuracy as a function of the number of PCs (or measurement parameters) retained.

A support vector machine (SVM) algorithm [24] was used as the classification technique. SVM is a classification algorithm based on statistical learning theory. The principal idea of an SVM is to determine an optimal separating hyperplane that maximizes the margin between two classes in a multidimensional data space. With the largest separation of the two data clusters, the SVM classifier gives a lower expected risk, which means that future error can be minimized if more data is added to the sample pool. Specifically, a linear kernel SVM classifier was employed in this study, and the classification was carried out on PCs retained from both fluorescence spectra and the diffuse reflectance spectrum or the diffuse reflectance spectrum only.

A full cross-validation of the algorithm was performed in the following manner. First, one sample was removed from the training dataset. The spectra of the remaining samples underwent the steps of preprocessing, PCA, Wilcoxon testing and SVM classification. The optimal PC scores (and corresponding eigenvectors) were identified from the Wilcoxon test and the optimal decision hyperplane was determined from the SVM analysis. Next, the optimized algorithm was applied to the sample that had been left out. In particular, the PC scores were calculated from the sample spectra using the optimal eigenvectors retained from the training set. Then, the sample was classified as malignant or nonmalignant based on which side of the optimal decision hyperplane its PC scores were distributed. This method allowed for an unbiased evaluation of the algorithm's performance when the sample size is too small to separate into independent training and testing data sets. This procedure was carried out for all of the 56 samples. For each testing sample, the algorithm was trained on the remaining 55 training samples.

In the original stages of algorithm development, a two-step algorithm was employed to differentiate between malignant and nonmalignant (normal and benign) tissues. This involved first discriminating between fibrous/glandular and adipose tissues and then discriminating between malignant and fibrous/glandular tissues. This step-wise approach resulted in samples being misclassified at each step. It was observed that a greater number of samples were misclassified using this approach relative to that in which the algorithm was used to directly discriminate between the two classes of interest i.e., malignant and nonmalignant (normal and benign) tissue. Therefore, the latter approach was employed in this study.

It is desirable to relate the PCs that contribute to optimal classification of malignant and nonmalignant breast tissues to features in the corresponding spectrum. This can be achieved by re-projecting the PCs back into the spectral data space. Re-projection of the PC of a given sample into the spectral data space can be achieved by multiplying the PC score of that sample by the corresponding eigenvector. A linear combination of the re-projected PCs that account for 100% of the variance can faithfully reconstruct the spectrum of that sample. Since the objective is to determine which spectral features are useful in the classification, only those PCs that showed the statistically most significant differences between malignant and nonmalignant tissues were used in the re-projection.

III. Results

Fig. 2 shows the average fluorescence excitation-emission matrices (EEMs) for malignant (20) [Fig. 2(a)], normal/benign fibrous (15) [Fig. 2(b)], and adipose tissues (21) [Fig. 2(c)]. Each EEM is shown on a log contour scale, where each contour corresponds to levels of equal fluorescence intensity. The useful fluorescence information is to the right of the Rayleigh scattering line seen in the upper left quadrant of the plot. This

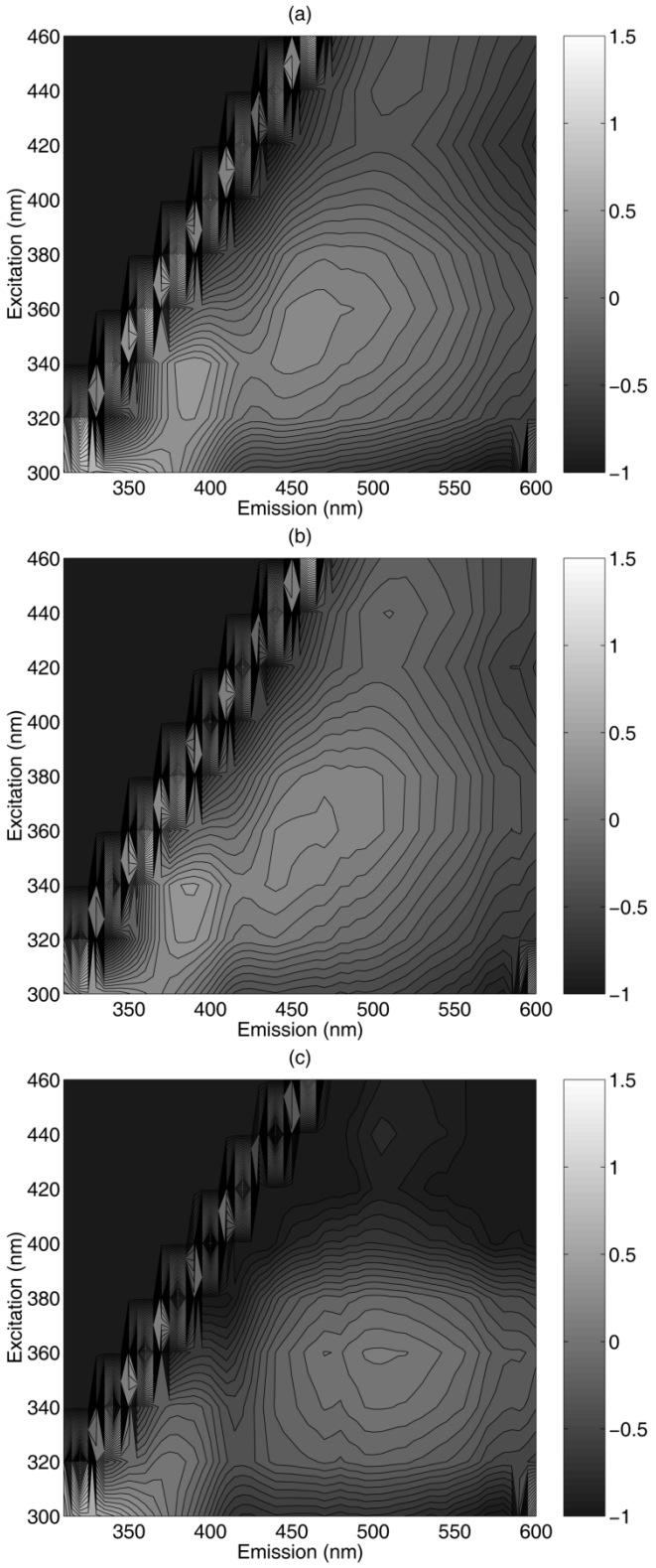

Fig. 2. Average fluorescence EEMs for (a) malignant ($n = 20$), (b) normal/benign fibrous ($n = 15$), and (c) adipose tissues ($n = 21$). Each EEM is shown on a log contour scale, where each contour corresponds to levels of equal fluorescence intensity. The useful fluorescence information is to the right of the Rayleigh scattering line seen in the upper left quadrant of the plot.

plot allows for the display of fluorescence intensities acquired at multiple excitation wavelengths where the fluorescence spectrum at each excitation wavelength corresponds to a horizontal slice through the plot. Four peaks are visible in the malignant [Fig. 2(a)] and normal/benign fibrous tissues [Fig. 2(b)], which occur in similar locations, i.e., at excitation, emission wavelength pairs of (300, 340), (340, 390), (360, 460), and (440, 520) nm. The adipose tissue EEM [Fig. 2(c)] on the other hand, shows distinct differences, relative to that observed in Fig. 2(a) and (b). Notably, the peak at (340, 390) nm is weakly present and the peak at (360, 460) nm has been shifted to approximately (360, 520) nm.

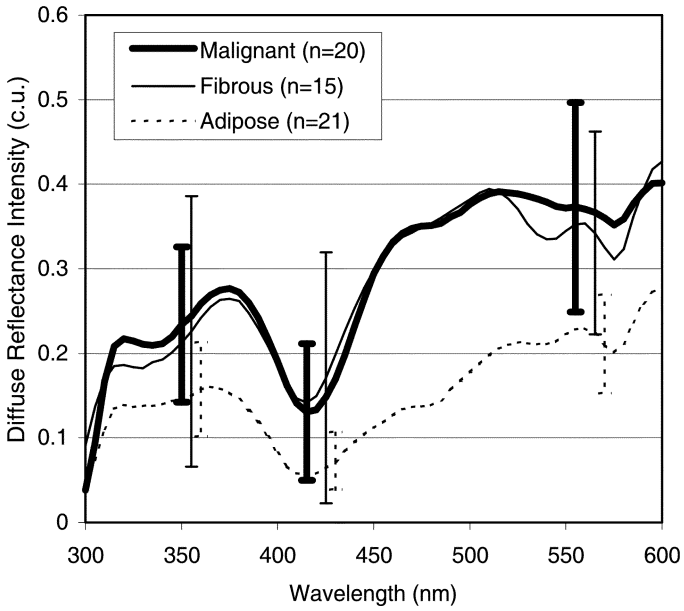

Fig. 3. Average diffuse reflectance spectra with standard deviations, for the malignant, normal/benign fibrous and adipose tissues.

Fig. 3 shows the average diffuse reflectance spectra with standard deviations for the malignant, normal/benign fibrous and adipose tissues. It can be seen that the average malignant and normal/benign fibrous tissue spectra have similar intensities, but subtle differences in spectral line shape in the wavelength regions between 300–350, 400–450 and 525–575 nm. The average adipose tissue spectrum shows decreased intensity at all wavelengths, and a distinctly different line shape between 425–525 nm compared to the average malignant and normal/benign fibrous tissue spectra. Note also that the variability in adipose tissue spectra is significantly less than that of fibrous and malignant tissues.

Table II shows the results of PCA, followed by a Wilcoxon rank-sum test for original [Table II(a)] and normalized [Table II(b)], fluorescence and diffuse reflectance spectra. The PCs that display differences between the malignant and nonmalignant tissues at different significance levels are listed. Each table is arranged to show which PCs meet a particular criterion but do not meet a higher criterion [for example in Table II(b), PC2 at 320-nm excitation meets both the $p < 0.05$ and $p < 0.005$ criterion but not $p < 0.0005$ criterion, and so is shown in the $p < 0.005$ column]. The PCs are organized based on which spectra they were derived from. For a particular spectrum, the PC number and the variance described by that PC (in parentheses) are indicated. Note that Table II shows the results of PCA and the Wilcoxon rank-sum test for all 56 samples.

TABLE II
THE RESULTS OF PCA, FOLLOWED BY A TWO-TAILED WILCOXON RANK-SUM TEST FOR (a) ORIGINAL AND (b) NORMALIZED FLUORESCENCE AND DIFFUSE REFLECTANCE SPECTRA. THE PCS THAT DISPLAY DIFFERENCES BETWEEN THE MALIGNANT AND NONMALIGNANT TISSUES AT DIFFERENT SIGNIFICANCE LEVELS ARE LISTED. EACH TABLE IS ARRANGED TO SHOW WHICH PCS MEET A PARTICULAR CRITERION BUT DO NOT MEET A HIGHER CRITERION (FOR EXAMPLE IN (B), PC2 AT 320 NM EXCITATION MEETS BOTH THE $p < 0.05$ AND $p < 0.005$ CRITERION BUT NOT $p < 0.0005$ CRITERION, AND SO IS SHOWN IN THE $p < 0.005$ COLUMN). THE PCS ARE ORGANIZED BASED ON WHICH SPECTRA THEY WERE DERIVED FROM. FOR A PARTICULAR SPECTRUM, THE PC NUMBER AND THE VARIANCE DESCRIBED BY THAT PC (IN PARENTHESES) ARE INDICATED. NOTE THAT TABLE II SHOWS THE RESULTS OF PCA AND THE WILCOXON RANK-SUM TEST FOR ALL 56 SAMPLES

Spectra	p<0.05	p<0.005	p<0.0005
300 nm Exc.	PC2 (0.06)		PC1 (0.93)
320 nm Exc.	PC1 (0.90)		
340 nm Exc.	PC1 (0.90)		
360 nm Exc.	PC1 ((0.89)		
380 nm Exc.	PC1 (0.97)		
400 nm Exc.	PC1 (0.991)		
420 nm Exc.	PC1 (0.995)		
440 nm Exc.	PC1 (0.996)		
460 nm Exc.	PC1 (0.997)		
Reflectance		PC1 (0.80)	

(a)

Spectra	p<0.05	p<0.005	p<0.0005
300 nm Exc.			PC2 (0.12)
320 nm Exc.	PC1 (0.72)	PC2 (0.17)	
340 nm Exc.	PC1 (0.95)		
360 nm Exc.	PC1 (0.75)		
380 nm Exc.	PC1 (0.77)		
400 nm Exc.		PC1 (0.68)	PC4 (0.02)
420 nm Exc.	PC3 (0.03)		PC1 (0.66)
440 nm Exc.		PC4 (0.02), PC1 (0.67)	
460 nm Exc.			PC3 (0.05)
Reflectance	PC3 (0.12), PC2 (0.37)		

(b)

A comparison of Table II(a) and (b) indicates that far more PCs at higher significance levels ($p < 0.005$ and $p < 0.0005$) are generated using normalized versus the original fluorescence spectra. Thus, this preprocessing method was utilized in all subsequent analysis of fluorescence spectra. It is interesting to note that both the original and normalized fluorescence spectra at 300-nm excitation yield PCs that meet the $p < 0.0005$ criterion. In Table II(b), it can be seen that as the significance level increases, the PCs that are retained from the fluorescence spectral data account for a smaller percent of the total variance. At a significance level of $p < 0.005$, the most useful fluorescence spectra are those measured at 300, 320, 400, 420, 440, and 460 nm excitation. In the case of the diffuse reflectance measurements, the original spectrum [Table II(a)] yields only one PC that meets the $p < 0.005$ criterion, while the normalized spectrum [Table II(b)] yields two PCs that meet the $p < 0.05$ criterion, but not the $p < 0.005$ criterion. Thus, both preprocessing methods were utilized in subsequent analysis of diffuse reflectance spectra.

PCs at higher significance levels are generated from fluorescence spectra than from the diffuse reflectance spectra. In Table II(a), there is one PC retained from the fluorescence spectrum at 300 nm, excitation, which is statistically more significant than the PC retained from the diffuse reflectance spectrum. In Table II(b), there are a total of seven PCs retained from fluorescence spectra at several excitation wavelengths that are statistically more significant than the two PCs retained from the diffuse reflectance spectrum.

In addition to the unpaired Wilcoxon rank-sum text, a Wilcoxon rank-signed test of normal/malignant PC pairs within the same patient was performed for a total of 11 normal/malignant tissue pairs. The Wilcoxon rank-signed test resulted in similar PCs to that generated from the Wilcoxon rank-sum test. Specifically, 11 of the 15 PCs identified as being significant from an unpaired analysis of normalized spectra [Table II(b)] were also identified as being significant from a paired analysis of the normalized spectra. The consistency between the paired and unpaired analysis confirms that the observed spectral differences between malignant and nonmalignant tissues are similar within and between patients.

Table III shows the classification results obtained from SVM analysis of the diagnostically important PCs derived from normalized spectra. The PCs used are similar to those indicated in Table II(b). However, it should be noted that Table II shows the results of PCA and the Wilcoxon rank-sum test for all 56 samples, while in the actual algorithm development, only 55 samples were used at a time in the training set (one testing sample was removed sequentially for the purposes of cross-validation). Thus, the PCs shown in Table II could vary slightly from those identified from the 56 independent training sets. The classification rate, sensitivity and specificity for the training and testing data sets are shown for PCs retained at progressively increasing levels of significance ranging from $p < 0.05$ to $p < 0.0005$. As seen in Table II(b), the PCs retained at the $p < 0.05$ significance level originate from both the fluorescence and diffuse reflectance spectra, while those retained at higher significance levels originate only from the fluorescence spectra. The PCs in the first three rows were identified from a set of PCs that describe 95% of the variance of the input data set. The PCs in the fourth row were identified from a set of PCs that describe 99% of the variance of the input data set. Increasing the percent variance from 95% to 99% results in two to three more PCs at the $p < 0.0005$ level. The training data set shows a classification accuracy (classification rate, sensitivity and specificity) that corresponds to the average and standard deviation of that obtained from training with a total of 56 data sets, each with a total of 55 samples (one sample at a time of a total of 56 samples was left out for the purposes of cross-validation). The classification accuracy of the testing data set reflects the unbiased performance of the algorithm on 56 samples through cross-validation.

Table III shows that cross-validation of the algorithm results in a 5%–20% decrease in the classification accuracy. It is interesting to note that the classification accuracy of the testing data set shows a smaller deviation relative to that of the training data set as the number of PCs used in the SVM analysis is reduced (by increasing the level of significance). Furthermore, the classification accuracy of testing data set increases slightly for increasing levels of significance. Selecting the diagnostically relevant PCs at the $p < 0.0005$ level of significance from a set of PCs that describe 99% as opposed to 95% of the variance of the input data set gives rise to an increase in the number of PCs used for SVM classification. This results in an improvement of the overall classification accuracy, as well as the smallest dif-

TABLE III

THE CLASSIFICATION RESULTS OBTAINED FROM SVM ANALYSIS OF THE DIAGNOSTICALLY IMPORTANT PCS DERIVED FROM NORMALIZED SPECTRA. THE CLASSIFICATION RATE, SENSITIVITY AND SPECIFICITY FOR THE TRAINING AND TESTING DATA SETS ARE SHOWN FOR PCS RETAINED AT PROGRESSIVELY INCREASING LEVELS OF SIGNIFICANCE RANGING FROM $p < 0.05$ TO $p < 0.0005$. AS SEEN IN TABLE II(b),THE PCS RETAINED AT THE $p < 0.05$ SIGNIFICANCE LEVEL ORIGINATE FROM BOTH THE FLUORESCENCE AND DIFFUSE REFLECTANCE SPECTRA, WHILE THOSE RETAINED AT HIGHER SIGNIFICANCE LEVELS ORIGINATE ONLY FROM THE FLUORESCENCE SPECTRA. THE PCS IN THE FIRST THREE ROWS WERE IDENTIFIED FROM A SET OF PCS THAT DESCRIBE 95% OF THE VARIANCE OF THE INPUT DATA SET. THE PCS IN THE FOURTH ROW (ASTERISKS) WERE IDENTIFIED FROM A SET OF PCS THAT DESCRIBE 99% OF THE VARIANCE OF THE INPUT DATA SET. THE TRAINING DATA SET SHOWS A CLASSIFICATION ACCURACY (CLASSIFICATION RATE, SENSITIVITY AND SPECIFICITY) THAT CORRESPONDS TO THE AVERAGE AND STANDARD DEVIATION OF THAT OBTAINED FROM TRAINING WITH A TOTAL OF 56 DATA SETS, EACH WITH A TOTAL OF 55 SAMPLES (ONE SAMPLE AT A TIME OF A TOTAL OF 56 SAMPLES WAS LEFT OUT FOR THE PURPOSES OF CROSS-VALIDATION). THE CLASSIFICATION ACCURACY OF THE TESTING DATA SET REFLECTS THE UNBIASED PERFORMANCE OF THE ALGORITHM ON 56 SAMPLES THROUGH CROSS-VALIDATION

Significance Level	Number of PCs	Classification Rate (%)		Sensitivity (%)		Specificity (%)	
		Training Data	Testing Data	Training Data	Testing Data	Training Data	Testing Data
P<0.05	14~15	91.53±2.76	75	84.16±5.66	65	95.60±2.10	80.56
P<0.005	7~8	86.95±1.87	76.79	77.36±4.65	65	92.27±3.06	83.33
P<0.0005	3~4	83.51±1.89	79	76.07±5.61	70	87.63±2.63	83.33
*P<0.0005	6~7	87.56±2.13	83.93	76.35±5.54	70	93.78±1.92	91.67

TABLE IV

CLASSIFICATION RESULTS OBTAINED FROM SVM ANALYSIS OF THE DIAGNOSTICALLY IMPORTANT PCS DERIVED FROM BOTH THE ORIGINAL AND NORMALIZED DIFFUSE REFLECTANCE SPECTRA. THIS IS A SIMILAR FORMAT TO TABLE III

Pre-processing	Significance Level	Number of PCs	Classification Rate (%)		Sensitivity (%)		Specificity (%)	
			Training Data	Testing Data	Training Data	Testing Data	Training Data	Testing Data
Original	P<0.1	2	66.62±2.51	60.71	45.43±8.85	30	78.38±1.73	77.78
Normalized	P<0.05	2	69.46±5.72	50	51.38±16.3	20	79.41±5.07	66.67

ference in the classification accuracy (in particular, the specificity) between the training and testing data sets. A comparison of the classification accuracy of PCs retained at the $p < 0.0005$ and $p < 0.05$ level of significance in Table III indicates that combining the normalized fluorescence and diffuse reflectance spectra does not improve the classification accuracy of an algorithm based on normalized fluorescence spectra alone.

Table IV shows classification results obtained from SVM analysis of the diagnostically important PCs derived from both the original and normalized diffuse reflectance spectra. This table has a similar format to Table III. Again the PCs selected for this analysis are similar to those shown in Table II. Table II shows that only one PC was retained from the original diffuse reflectance spectra [Table II(a)] and two PCs were retained from the normalized diffuse reflectance spectra [Table II(b)] when a criterion of $p < 0.05$ was used. In order to carry out SVM analysis, at least two features (PCs) are needed. Thus, the $p < 0.1$ criterion was used in order to select at least two diagnostically relevant PCs from the original diffuse reflectance spectra.

Table IV shows that cross-validation of the algorithm results in a 10%–30% decrease in the classification accuracy. The classification accuracy of the testing data set shows a smaller deviation relative to that of the training data set for PCs derived from the original diffuse reflectance spectra. In addition, the classification accuracy of testing data set for PCs extracted from the original spectra is higher than that for PCs derived from the normalized spectra. A comparison of the classification accuracy of PCs retained at the $p < 0.05$ or $p < 0.1$ level of significance in Table IV and $p < 0.0005$ level of significance in Table III indicates that using normalized fluorescence spectra yields significantly higher classification accuracy than using either the original or normalized diffuse reflectance spectra alone.

Fig. 4 shows the average normalized fluorescence spectra at 300-nm excitation [Fig. 4(a)] and the average spectral representations reflected by PC2 (which was obtained from the normalized fluorescence spectra at 300 nm, excitation), for malignant and nonmalignant tissues, and the difference spectra (between malignant and nonmalignant tissues) for each case [Fig. 4(b)]. The spectral representations are re-projections from the PC subspace onto the normalized spectral data space. They are calculated by simply multiplying the PC scores (in this case, PC2) for all samples by the associated eigenvector and then averaging the spectral representations for each tissue type (malignant and nonmalignant). The difference spectrum was obtained by subtracting (point-by-point) the average nonmalignant spectrum from the average malignant spectrum. PC2 was selected for the spectral representation because the Wilcoxon rank-sum test indicated that PC2 displays the statistically most significant differences between malignant and nonmalignant tissues. It should be pointed out that although PC1 accounts for more of the variance in the spectral data than PC2, it also reflects the variance present in both malignant and nonmalignant tissues.

In Fig. 4(a), the average normalized fluorescence spectrum of the malignant tissues shows a red shift in the fluorescence peak and a lower intensity between 450–550 nm relative to nonmalignant tissues. These differences are reflected in the average spectral representation of the malignant and nonmalignant tissues. The differences seen in the average malignant and nonmalignant tissue spectral representations track the differences observed in their corresponding average normalized fluorescence spectra, but do not necessarily replicate the actual spectra itself, since only one PC is used in the re-projection. Fig. 4(b) shows the difference spectra (between malignant and nonmalignant tissues) for both the average normalized spectra and average spectral representations shown in Fig. 4(a). It can be seen that the two difference spectra are very similar to each other, as expected. This verifies that PC2 displays the most significant difference between the two tissue types. The difference spectra indicate that the most significant differences between malignant and nonmalignant tissues are observed near emission wavelengths of 350 and 500 nm, when an excitation wavelength

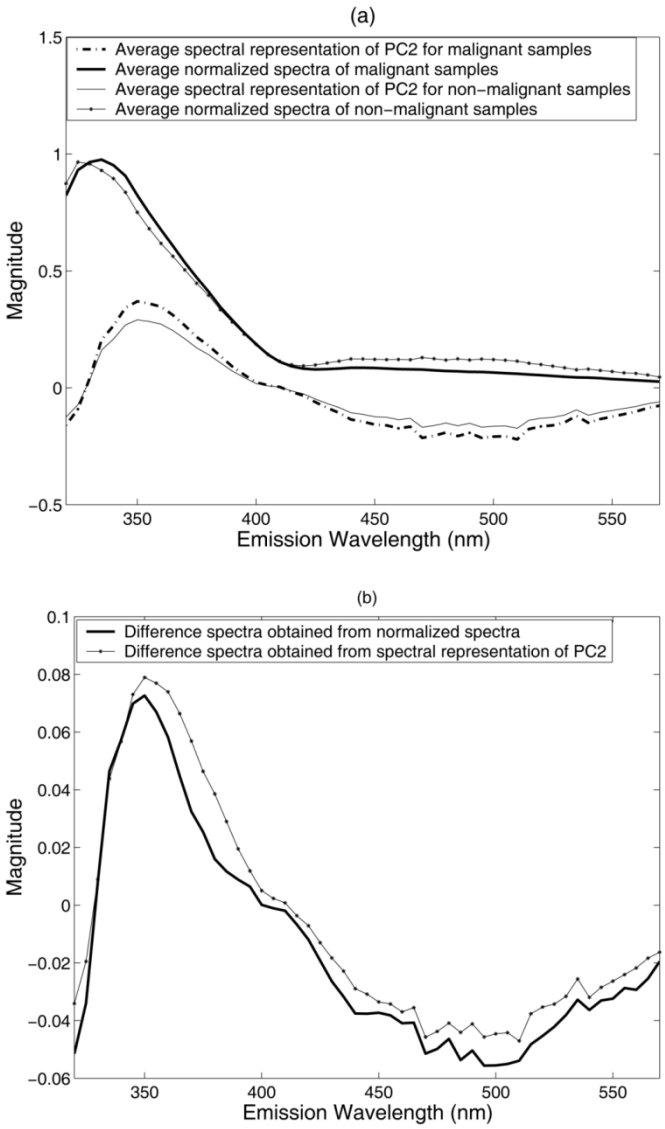

Fig. 4. (a) The average normalized fluorescence spectra at 300 nm, excitation, and the average spectral representations reflected by PC2 (which was obtained from the normalized fluorescence spectra at 300 nm, excitation), for malignant and nonmalignant tissues, and (b) the difference spectra (between malignant and nonmalignant tissues) for each case. The spectral representations are re-projections from the PC subspace onto the normalized spectral data space. They are calculated by simply multiplying the PC scores (in this case, PC2) for all samples by the associated eigenvector and then averaging the spectral representations for each tissue type (malignant and nonmalignant). The difference spectrum was obtained by subtracting (point-by-point) the average nonmalignant spectrum from the average malignant spectrum.

of 300 nm is used. Spectral representations obtained from PC4 at 400-nm excitation, and PC3 at 460-nm excitation are not shown here, but indicate that the maximal differences between malignant and nonmalignant tissues are observed at emission wavelengths of 460 and 540 nm, respectively.

IV. Discussion

Optical spectroscopy in the UV-VIS spectral range is demonstrated to be useful in discriminating malignant and nonmalignant human breast tissues. By measuring fluorescence spectra at multiple excitation wavelengths as well as diffuse reflectance spectra and performing a separate analysis on each, those spectra that are most useful in discriminating malignant and nonmalignant tissues were identified. The analysis indicated that only four of the ten measured spectra are required to maximize classification accuracy. These include fluorescence spectra at excitation wavelengths of 300, 400, 420, and 460 nm. This has important implications in clinical applications, where both speed and cost are important, in that the fewer wavelengths that have to be measured, the faster and less complex the instrument can be.

One problem with the particular approach employed here for analysis is that it can be difficult to determine the biological basis of the differences observed in the fluorescence spectra of malignant and nonmalignant tissues. However, an understanding of the fluorophores that contribute to the fluorescence spectra at the four optimal excitation wavelengths can yield some insight into the sources of endogenous contrast present. The excitation wavelengths used, ranging from 300 to 460 nm, allow for the characterization of a number of fluorophores, including tryptophan, NAD(P)H, flavoproteins and collagen [17]. By using a range of excitation wavelengths, one is able to characterize many or all of the biological fluorophores present in breast tissue. The fluorescence excitation-emission wavelengths identified as being diagnostic from the PCA-SVM algorithm suggest that the important fluorophores for breast cancer diagnosis are tryptophan, collagen, NADH and flavoproteins. This qualitative analysis does not preclude the possibility that the differences in the fluorescence spectra of malignant and nonmalignant tissues may also be influenced by the absorption of hemoglobin.

As discussed previously, the fluorescence spectra at 300 nm, excitation appear to be most diagnostic of breast cancer. Fig. 4 shows a red shift in the fluorescence peak at 340 nm (tentatively assigned to tryptophan fluorescence), and a decrease in fluorescence at the smaller peak occurring around 450-nm emission (tentatively assigned to NADH fluorescence) in the malignant samples, relative to nonmalignant tissues. This finding is consistent with previous work by Yang. *et al.* [10], who found that at an excitation wavelength of 300 nm, the fluorescence emission peak at 340 nm was red-shifted for malignant samples relative to that of normal adipose tissues and the fluorescence at around 450-nm emission was decreased in malignant relative to fibrous tissues. It may be that the shifted peak is useful in discriminating the malignant tissues from adipose, and that the decreased fluorescence at 450 nm is useful in discriminating malignant tissue from benign fibrous tissues, and so the combination of the two features makes this particular PC useful in discriminating malignant and nonmalignant tissues.

Diffuse reflectance can characterize some of the same optical features exploited in fluorescence spectroscopy, notably absorption due to various biological chromophores, and tissue scattering properties. The primary absorbers are oxygenated and deoxygenated hemoglobin, which are present in blood. These compounds, which have slightly different absorption spectra, can be used as an indicator of tissue oxygenation [17]. β-carotene is another chromophore and is present in adipose tissues, thus providing a unique indicator of this tissue type. The primary advantage of this technique is that diffuse reflectance signals are several orders of magnitude greater than the weak endogenous fluorescence signals measured from tissue. Therefore, if diffuse reflectance measurements were

capable of discriminating malignant and nonmalignant tissues at similar accuracies to that of fluorescence measurements, there would be a considerable increase in cost-effectiveness. However, using a similar classification technique, diffuse reflectance spectroscopy was not capable of discriminating between malignant and nonmalignant tissues with the same accuracy as fluorescence spectroscopy. Therefore, there is an apparent advantage to using fluorescence in addition to, or instead of diffuse reflectance. This advantage is likely due to the additional chemical specificity that arises from the fluorescence characterization of the many biologic fluorophores intrinsically present in tissue.

Bigio *et al.* reported better classification accuracies for discriminating between malignant and nonmalignant breast tissues using diffuse reflectance spectroscopy in a pilot study [16], as well as in a more recently published abstract [25]. However, it is difficult to compare classification accuracies achieved in our study to that carried out by Bigio and co-workers due to differences in the clinical protocol (the studies by Bigio and co-workers were carried out on tissues *in vivo*), probe geometry, spectral range (the spectral measurements were made from 330–750 nm) and methods of analysis employed in the two studies. What can be concluded from the work presented here is that fluorescence spectroscopy provides superior classification accuracy compared to diffuse reflectance spectroscopy when evaluated on the same samples using the same methods of analysis.

A novel nonparametric algorithm was developed to identify and incorporate the optimal spectral features for discriminating between malignant and nonmalignant breast tissues. The use of the Wilcoxon test and SVM classification scheme does not require *a priori* knowledge about the sample distribution and thus, can be utilized for the analysis of small sample sizes. Cross-validation of the algorithm highlights the importance of obtaining an unbiased estimate of the algorithm's classification accuracy. Cross-validation techniques may indicate that the training data set is not sufficient to fully characterize the variance of each subgroup (malignant and nonmalignant tissues). Thus, by removing one data point, the decision hyperplane is altered enough to misclassify some additional samples. Indeed, in examining the misclassified samples, it is clear that some underrepresented sub-groups of tissue types are most frequently misclassified. There were five malignant samples that were consistently misclassified (once in cross validation and repeatedly in the training set). Of these five samples two were carcinoma *in situ* (CIS) and two were lobular cancers. These samples represent the total number of CIS and lobular cancers in the entire sample pool. Upon cross-validation, one of these samples would be removed prior to training the algorithm, leaving just one other sample of this type to aid in its classification. Thus, the total variance accounted for by these types of cancers is not well represented in the training set, which results in the frequent misclassification of these particular cancers. Upon the inclusion of more data points from these sample types, the unbiased (testing) classification accuracy may approach the accuracy achieved with the training data set.

Typically, the optical spectral features of different tissue types are not fully separable, which gives rise to imperfect classification. The classification accuracy is also dependent on the algorithm used. Given a constant sample size, one approach to improving the classification accuracy may be to incorporate more features into the classifier (such as PCs). As depicted in Table IV, increasing the number of inputs did not significantly improve the classification accuracy. An alternative approach to improving the classification accuracy is to use nonlinear rather than the linear methods of analysis employed here, i.e., PCA and linear SVM. For example, using a nonlinear kernel in SVM classification may improve the classification accuracy, since the nonlinear kernel SVM is expected to be superior to the linear kernel in dealing with nonseparable cases. This is beyond the scope of the current study, but will be explored in future investigations.

One of the goals of future work is to carry out clinical studies to explore the effectiveness of optical spectroscopy for detecting breast cancer during core needle biopsy. In particular, side-firing fiber-optic probes will be designed and fabricated for use in a Mammatome core biopsy needle. The tip of the needle has a side-facing aperture (19 mm long and 2 mm wide), through which pieces of tissue can be vacuum suctioned when the needle is inserted into the breast. The side-firing probes can be incorporated into the needle to measure fluorescence and diffuse reflectance spectra of breast tissues after the needle is positioned in the area of concern in the breast, but before biopsy. The diagnosis based on the spectral features can be compared to histology of the corresponding biopsy to evaluate the diagnostic potential of this technique.

It would also be desirable to gain a quantitative understanding of the biological basis for the observed spectral differences, which are difficult to determine directly from the tissue spectra. As such, the use of systems employing cell lines and tissue cultures are being explored. A stepwise approach to this technology is warranted, starting with simple systems and adding additional levels of complexity. For example, a normal and malignant cell monolayer could first be imaged to establish the intrinsic fluorescence properties of these cell types. Then the same cells could be grown in a 3-D collagen matrix, adding the effects of the interaction with the extracellular matrix. Finally, these cells could be implanted into nude mice models to explore the added effects of the vasculature and adipose tissue. Such a stepwise approach could allow one to compare simpler, better understood models to what has been characterized in tissue, and could perhaps allow one to determine what tissue constituent is most responsible for the observed spectral differences. This is a promising avenue of research, and applied to the breast could allow for an increased understanding of the underlying mechanism for how optical spectroscopy is able to diagnose this disease.

REFERENCES

[1] J. R. Harris, M. E. Lippman, M. Morrow, and C. K. Osborne, *Diseases of the Breast*, 2nd ed. Philadelphia, PA: Lippicott Williams & Wilkins, 2000.

[2] R. J. Jackman, K. W. Nowels, J. Rodriguez-Soto, F. A. Marzoni Jr, S. I. Finkelstein, and M. J. Shepard, "Stereotactic, automated, large-core needle biopsy of nonpalpable breast lesions: False-negative and histologic underestimation rates after long-term follow-up," *Radiology*, vol. 210, no. 3, pp. 799–805, 1999.

[3] D. D. Dershaw, E. A. Morris, L. Liberman, and A. F. Abramson, "Nondiagnostic stereotaxic core breast biopsy: Results of rebiopsy," *Radiology*, vol. 198, no. 2, pp. 323–5, 1996.

[4] J. E. Meyer, D. N. Smith, S. C. Lester, P. J. DiPiro, C. M. Denison, S. C. Harvey, R. L. Christian, A. Richardson, and W. D. Ko, "Large-needle core biopsy: Nonmalignant breast abnormalities evaluated with surgical excision or repeat core biopsy," *Radiology*, vol. 206, no. 3, pp. 717–720, 1998.
[5] N. Ramanujam, "Fluorescence spectroscopy of neoplastic and nonneoplastic tissues," *Neoplasia*, vol. 2, no. 1–2, pp. 89–117, 2000.
[6] S. K. Majumder, P. K. Gupta, B. Jain, and A. Uppal, "UV excited autofluorescence spectroscopy of human breast tissues for discriminating cancerous tissue from benign tumor and normal tissue," *Lasers Life Sci.*, vol. 8, no. 4, pp. 249–264, 1999.
[7] P. K. Gupta, S. K. Majumder, and A. Uppal, "Breast cancer diagnosis using N2 laser excited autofluorescence spectroscopy," *Lasers Surg. Med.*, vol. 21, no. 5, pp. 417–242, 1997.
[8] Y. Yuanlong, E. J. Celmer, M. Zurawska-Szczepaniak, and R. R. Alfano, "Excitation spectrum of malignant and benign breast tissues: A potential optical biopsy approach," *Lasers Life Sci.*, vol. 7, no. 4, pp. 249–265, 1997.
[9] Y. Yang, A. Katz, E. J. Celmer, M. Zurawska-Szczepaniak, and R. R. Alfano, "Fundamental differences of excitation spectrum between malignant and benign breast tissues," *Photochem. Photobiol.*, vol. 66, no. 4, pp. 518–522, 1997.
[10] ——, "Optical spectroscopy of benign and malignant breast tissues," *Lasers Life Sci.*, vol. 7, no. 2, pp. 115–27, 1996.
[11] R. R. Alfano, A. Pradhan, G. C. Tang, and S. J. Wahl, "Optical spectroscopic diagnosis of cancer and normal breast tissues," *J. Opt. Soc. Amer. B (Opt. Phys.)*, vol. 6, no. 5, pp. 1015–1023, 1989.
[12] R. R. Alfano, G. C. Tang, A. Pradhan, W. Lam, D. S. J. Choy, and E. Opher, "Fluorescence spectra from cancerous and normal human breast and lung tissues," *IEEE J. Quantum Electron.*, vol. QE-23, pp. 1806–1811, Oct. 1987.
[13] Y. Yang, E. J. Celmer, J. A. Koutcher, and R. R. Alfano, "UV reflectance spectroscopy probes DNA and protein changes in human breast tissues," *J. Clin. Laser Med. Surg.*, vol. 19, no. 1, pp. 35–39, 2001.
[14] N. Ghosh, S. K. Mohanty, S. K. Majumder, and P. K. Gupta, "Measurement of optical transport properties of normal and malignant human breast tissue," *Appl.-Optics*, vol. 40, no. 1, pp. 176–84, 2001.
[15] S. V. Pushkarev, S. A. Naumov, S. M. Vovk, V. A. Volovodenko, and V. V. Udut, "Application of laser fluorescence spectroscopy and diffuse reflection spectroscopy in diagnosing the states of mammary gland tissue," *Optoelectron., Instrum. Data-Processing*, vol. 2, pp. 71–76, 1999.
[16] I. J. Bigio, S. G. Bown, G. Briggs, C. Kelley, S. Lakhani, D. Pickard, P. M. Ripley, I. G. Rose, and C. Saunders, "Diagnosis of breast cancer using elastic-scattering spectroscopy: Preliminary clinical results," *J. Biomed. Opt.*, vol. 5, no. 2, pp. 221–228, 2000.
[17] N. Ramanujam, "Fluorescence spectroscopy in vivo," in *Encyclopedia of Analytical Chemistry*, R. Meyers, Ed. New York: Wiley, 2000, pp. 20–56.
[18] Y. Yang, E. J. Celmer, J. A. Koutcher, and R. R. Alfano, "DNA and protein changes caused by disease in human breast tissues probed by the Kubelka-Munk spectral functional," *Photochem. Photobiol.*, vol. 75, no. 6, pp. 627–632, 2002.
[19] G. M. Palmer, C. L. Marshek, K. M. Vrotsos, and N. Ramanujam, "Optimal methods for fluorescence and diffuse reflectance measurements of tissue biopsy samples," *Lasers Surg. Med.*, vol. 30, no. 3, pp. 191–200, 2002.
[20] Q. Liu, C. Zhu, and N. Ramanujam, "Experimental validation of Monte Carlo modeling of fluorescence in tissues in the UV-visible spectrum," *J. Biomed. Opt.*, vol. 8, 2003.
[21] J. A. Welch and J. C. M. Van Gemert, *Optical-Thermal Response of Laser-Irradiated Tissue*. New York: Plenum, 1995.
[22] R. A. Johnson and D. W. Wichern, *Applied Multivariate Statistical Analysis*. Englewood Cliffs, N.J: Prentice-Hall, 1982.
[23] R. M. Bethea, B. S. Duran, and T. L. Boullion, *Statistical Methods for Engineers and Scientists*, 3rd ed., M. Dekker, Ed. New York, 1995.
[24] C. Burges, "A tutorial on support vector machines for pattern recognition," *Data Mining and Knowledge Discovery*, vol. 2, no. 2, pp. 121–167, 1998.
[25] A. C. Lee, C. D. O. Pickard, M. R. S. Keshtgar, G. M. Briggs, M. Falzon, S. Lakhani, I. Bigio, and S. G. Bown, "Elastic scattering spectroscopy for the diagnosis of breast cancer," *Br. J. Surg.*, vol. 89, no. Suppl. 1, pp. 74–74, 2002.

Gregory M. Palmer is a graduate student in the Department of Biomedical Engineering at the University of Wisconsin, Madison. He received the B.S. degree in biomedical engineering from Marquette University, Milwaukee, WI, in June, 2000, and the M.S. degree from the University of Wisconsin, Madison, in December 2002. He is presently working toward his doctorate at the same school.

Mr. Palmer is a member of SPIE.

Changfang Zhu received the B.S. degree in biomedical engineering from the Zhejiang University, Hangzhou, China, in 1998, and the M.S. degree in biomedical engineering from Tsinghua University, Beijing, China, in 2001. She is currently working towards the Ph.D. degree in electrical engineering at the University of Wisconsin, Madison.

Ms. Zhu is a member of the SPIE.

Tara M. Breslin is an Assistant Professor in the Section of Surgical Oncology at the University of Wisconsin Medical School, Madison. Her research interests include clinical trials in breast cancer technology and development in breast cancer diagnosis and treatment.

Dr. Breslin is a member of the Society of Surgical Oncology, the Fellow American College of Surgeons, and the American College of Surgeons Oncology Group.

Fushen Xu is an Instructor with the Department of Pathology and Laboratory Medicine at the University of Wisconsin Medical School, Madison.

Kennedy W. Gilchrist is a Professor of Pathology and Laboratory Medicine at the University of Wisconsin Medical School, Madison. His primary research interests involve aspects of breast cancer care.

Dr. Gilchrist is a member of the Eastern Cooperative Oncology Group, and is on the Editorial Board of *Breast Cancer Research and Treatment*.

Nirmala Ramanujam received the Ph.D. degree in biomedical engineering from the University of Texas, Austin, in 1995. Her area of specialization was in biomedical optical spectroscopy.

She was awarded the National Research Service Award from the NIH to do a Postdoctoral fellowship at the University of Pennsyslania (UPENN), Philadelphia, and following this fellowship, she worked as an Assistant Professor in the Department of Biochemistry and Biophysics at UPENN. In 2000, she joined the University of Wisconsin, Madison, as an Assistant Professor of Biomedical Engineering. Her current research interests are centered on developing optical diagnostic modalities for breast cancer.

Dr. Ramanujam is a member of OSA, SPIE, APS, ASLMS, and ASEE.